RESEARCH ARTICLE

Proteomic analysis of sheep primary testicular cells infected with bluetongue virus

*Junzheng Du[1], Shanshan Xing[1], Zhancheng Tian[1], Shandian Gao[1], Junren Xie[1], Huiyun Chang[1], Guangyuan Liu[1], Jianxun Luo[1] and Hong Yin[1,2]**

[1] State Key Laboratory of Veterinary Etiological Biology, Lanzhou Veterinary Research Institute, Chinese Academy of Agricultural Sciences, Lanzhou, Gansu, P. R. China
[2] Jiangsu Co-innovation Center for Prevention and Control of Important Animal Infectious Diseases and Zoonoses, Yangzhou, P. R. China

Received: July 7, 2015
Revised: January 3, 2016
Accepted: March 11, 2016

Bluetongue virus (BTV) causes a non-contagious, arthropod-transmitted disease in wild and domestic ruminants, such as sheep. In this study, we used iTRAQ labeling coupled with LC-MS/MS for quantitative identification of differentially expressed proteins in BTV-infected sheep testicular (ST) cells. Relative quantitative data were obtained for 4455 proteins in BTV- and mock-infected ST cells, among which 101 and 479 proteins were differentially expressed at 24 and 48 h post-infection, respectively, indicating further proteomic changes during the later stages of infection. Ten corresponding genes of differentially expressed proteins were validated via real-time RT-PCR. Expression levels of three representative proteins, eIF4a1, STAT1 and HSP27, were further confirmed via western blot analysis. Bioinformatics analysis disclosed that the differentially expressed proteins are primarily involved in biological processes related to innate immune response, signal transduction, nucleocytoplasmic transport, transcription and apoptosis. Several upregulated proteins were associated with the RIG-I-like receptor signaling pathway and endocytosis. To our knowledge, this study represents the first attempt to investigate proteome-wide dysregulation in BTV-infected cells with the aid of quantitative proteomics. Our collective results not only enhance understanding of the host response to BTV infection but also highlight multiple potential targets for the development of antiviral agents.

Keywords:
BTV / Differential expression / iTRAQ / Microbiology / Quantitative proteomics

Additional supporting information may be found in the online version of this article at the publisher's web-site

1 Introduction

Bluetongue (BT) is a non-contagious, arthropod-transmitted disease of wild and domestic ruminants, such as sheep, goats, cattle, buffaloes, camel and deer. Infection is enzootic in many tropical and temperate regions, coincident with the distribution of biting midges (*Culicoides spp*) [1–3]. BT is listed as a 'notifiable' disease by the Office International des Epizooties (OIE) [4]. The virus responsible for BT is classified within the prototype species *bluetongue virus* (BTV) of *Orbivirus*, the largest genus within the family *Reoviridae*. The genome of BTV consists of ten segments of double-stranded RNA encoding seven structural (VP1 to VP7) and four non-structural (NS1 to NS4) proteins [5–7]. Twenty-seven distinct BTV serotypes (BTV1 to BTV27) induce serotype non-cross

Correspondence: Dr. Junzheng Du, State Key Laboratory of Veterinary Etiological Biology, Lanzhou Veterinary Research Institute, Chinese Academy of Agricultural Science, Xujiaping 1, Lanzhou, Gansu, 730046, P. R. China
E-mail: dujunzheng@caas.cn

Abbreviations: **BTV**, bluetongue virus; **CPE**, cytopathic effect; **hpi**, hours postinfection; **NPCs**, nuclear pore complexes; **PCV2**, porcine circovirus type 2; **PFU**, plaque formation units; **ST**, sheep testes; **UPS**, ubiquitin-proteasome system

*Additional corresponding author: Professor Hong Yin E-mail: yinhong@caas.cn
Colour Online: See the article online to view Figs. 1, 2, 3, 5 in colour.

Significance of the study

Proteomic approaches are increasingly recognized as effective tools facilitating comprehensive characterization of virus–host cell interactions. Although BTV, a prototype of the genus *Orbivirus* within the family *Reoviridae*, has been extensively studied, the interactions between virus and host cells are not fully understood at present. In this study, we investigated proteomic alterations in BTV-infected ST cells using iTRAQ labeling combined with LC−MS/MS for the first time. The identification of significantly altered proteins in BTV-infected ST cells provides a global overview of the BTV–host cell interaction network. Many of the immune response-related proteins differentially expressed upon BTV infection are novel and have not been reported to date. Elucidation of the functions of these proteins in virus–host cell interactions may be useful for the development of new therapeutic strategies targeting BTV.

protective immunity and have an impact on vaccination strategies [3, 8]. BTV usually causes severe haemorrhage and ulceration of the mucous membranes in ruminants, along with fever, lameness, coronitis, pulmonary oedema, swelling of the head (particularly lips and tongue) and death. In this regard, the pathogenesis of bluetongue is similar to that of hemorrhagic viral fevers of humans, such as Ebola virus [2, 9, 10].

At least eight different serotypes of BTV (BTV-1, 2, 4, 6, 8, 9, 11 and 16) have emerged in Europe since 1998, collectively representing the largest outbreak of the disease ever recorded that led to the deaths of over 1.8 million animals [11–13]. BTV caused significant mortality, estimated at ~50% and 15% in clinically affected sheep and cattle, respectively, during the northern European outbreak in 2006–2008 [9, 14]. As a result of its economic importance, BTV has been studied extensively as a model system for related viruses, and represents one of the most well characterized viruses [5, 15, 16].

Although the mechanisms of BTV action have been elucidated, the interactions between virus and host cells are not fully understood at present [2, 5, 15]. Proteomic approaches provide effective tools for the comprehensive characterization of virus–host interactions and identification of the cellular proteins involved directly or indirectly in viral infection via detection of the relative changes in protein expression [17–19]. For example, two-dimensional gel electrophoresis (2DE) and matrix-assisted laser desorption-ionization time-of-flight tandem mass spectrometry (MALDI-TOF/MS) proteomic approaches have been employed to investigate proteomic changes in host cells in response to virus infections, including classical swine fever virus [20], infectious bursal disease virus [21], severe acute respiratory syndrome associated coronavirus [22] and porcine circovirus type 2 (PCV2) [23]. Stable isotope labeling of amino acids in cell culture (SILAC) and mass spectrometry (MS) have additionally been employed for characterization of pathogenic viruses, including PCV2 [24], influenza virus [25], adenovirus [26], Japanese encephalitis virus [27] and human immunodeficiency virus [28]. These studies have provided extensive insights into the infected host cell proteomes and enhanced our understanding of the alterations induced in signaling pathways in response to viral infection.

iTRAQ is a more sensitive and accurate technique than traditional proteomic approaches (2DE, MALDI-TOF/MS and SILAC) for quantifying low-abundance proteins. The method has been employed to investigate virus–host interactions for several viral pathogens, such as transmissible gastroenteritis virus [29], porcine reproductive and respiratory syndrome virus [30], PCV2 [31], porcine epidemic diarrhea virus [32] and equine infectious anemia virus [33]. The mechanisms of BTV pathogenesis and immunomodulation have not been established to date. In the present study, we investigated the host cell response by profiling changes in cellular protein expression patterns in BTV-infected cells using iTRAQ labeling combined with liquid chromatography-mass spectrometry (LC−MS/MS). Alterations in protein expression levels were verified using quantitative real-time RT-PCR and western blot analyses. The possible biological significance of the differentially expressed proteins identified in the host response to BTV infection was further evaluated using bioinformatics tools.

2 Materials and methods

2.1 Cells and viruses

Sheep testes (ST) cells were obtained from three healthy 2 week-old male lambs. Briefly, testes were collected and washed with phosphate-buffered saline (PBS, pH 7.4) supplemented with 100 U/mL penicillin and 100 μg/mL streptomycin. Testicular tissues were cut into small pieces and digested with trypsin at 37°C for 30 min. Isolated ST cells were washed with PBS three times and resuspended in RPMI-1640 (Hyclone, USA) supplemented with 15% fetal bovine serum (Gibco, USA). Cells were seeded into tissue culture flasks (Corning, USA) at a density of 1×10^5 cells/mL and incubated at 37°C under 5% CO_2 for ~1–2 days. Non-adherent and loosely adherent cells were removed by mildly shaking flasks before changing the medium, and the remaining adherent cells further incubated for 3–4 days. The BTV-1 strain (GS/11) was isolated in western China and propagated in BHK-21 cells (ATCC-CCL-10) obtained from the American Type Culture Collection. The viral titer, determined using a

plaque formation assay on a monolayer of BHK-21 cells, was estimated as plaque formation units per milliliter (PFU/mL) [16]. All animal experiments were performed according to the protocols approved by the Animal Care and Use Committee of the Lanzhou Veterinary Research Institute (permit no. 2009–26). All experiments with infectious viruses were conducted in Biosafety Level 3 facilities.

2.2 Virus inoculation

The monolayer of confluent ST cells was dispersed with 0.25% trypsin and 0.02% EDTA and seeded in 6 cm cell culture flasks. After a 24 h incubation period, the culture medium was removed and ST cells washed with PBS. Cells were inoculated with BTV-1 at a multiplicity of infection (MOI) of 0.1. After 1 h of adsorption, infected cells were maintained in RPMI-1640 supplemented with 2% FBS. Uninfected ST cells were used as the mock-infected group. Viral propagation was confirmed with cytopathic effect (CPE) and one-step growth curve of BTV-1 in BHK-21 cells. Three replicates of virus- and mock-infected cultures were prepared at each time-point. The CPE was observed under a light microscope at 0, 12, 24, 48, and 72 hours post infection (hpi). To further confirm BTV infection in ST cells, RT-PCR was performed using the S7F (5′-GTTAAAAATCTATAGAGATGG-3′) and S7R (5′-GTAAGTGTAATCTAAGAG-3′) primers to detect the viral S7 gene. Total RNA was extracted using TRIzol (Invitrogen, USA) according to the manufacturer's instructions, and RT-PCR performed with the one-step PrimeScript RT reagent Kit (Takara, Japan). PCR products were verified using 1% agarose gel electrophoresis and sequenced using an ABI Prism 377 DNA sequencer (Applied Biosystems, USA).

2.3 Protein preparation

BTV-infected and mock-infected ST cells in 25 cm^2 flasks (3×10^6 cells/flask) were collected at 24 and 48 hpi with a cell scraper, centrifuged at 1000 × *g* for 5 min, and washed three times with ice-cold PBS. Three batches of ST cells were prepared from three lambs, and each batch infected with BTV-1 or mock infected for 24 and 48 h. Equal amounts of cells from each of the three batches of virus- and mock-infected cells were mixed at each time-point. Mixed cell pellets were suspended in lysis buffer (7 M Urea, 2 M Thiourea, 4% CHAPS, 40 mM Tris-HCl, pH 8.5, 1 mM PMSF, 2 mM EDTA) and sonicated at 200 watts for 5 min on ice. Proteins were reduced with 10 mM DTT, alkylated with 55 mM iodoacetamide for 1 h, and subsequently precipitated using chilled acetone. After centrifugation at 4°C and 30 000 × *g*, the pellet was dissolved in 0.5 M TEAB (Applied Biosystems, Italy) and sonicated on ice. Following another centrifugation step at 30 000 × *g* and 4°C, an aliquot of supernatant was obtained for determination of protein concentration with the Bradford protein assay using the 2-D Quant kit (Amersham, USA). Proteins in the supernatant were stored at –80°C for further analysis.

2.4 iTRAQ labeling and fractionation with SCX chromatography

An aliquot of total protein (100 μg) was obtained from each sample solution and digested with Trypsin Gold (Promega, Madison, WI, USA) at a trypsin/protein ratio of 1:30 at 37°C overnight. Peptides were dried via vacuum centrifugation, reconstituted in 0.5 M TEAB, and processed according to the manufacturer's protocol for 8-plex iTRAQ reagent labeling. Peptides prepared from BTV- and mock-infected ST cells at 24 hpi were labeled with iTRAQ tag 114 and iTRAQ tag 116, while those prepared from BTV- and mock-infected ST cells at 48 hpi were labeled with iTRAQ tag 118 and iTRAQ tag 119, respectively. Labeled peptide mixtures were pooled and dried via vacuum centrifugation.

SCX chromatography was performed with a LC-20AB HPLC Pump system (Shimadzu, Japan). iTRAQ-labeled peptide mixtures were resuspended with 4 mL buffer A (25 mM NaH_2PO_4 in 25% ACN, pH 2.7) and loaded onto a 4.6×250 mm Ultremex SCX column containing 5 μm particles. Peptides were eluted with a gradient of buffer A for 10 min, 5–60% buffer B (25 mM NaH_2PO_4, 1 M KCl in 25% ACN, pH 2.7) for 27 min, and 60–100% buffer B for 1 min at a flow rate of 1 mL/min. Elution was monitored by measuring absorbance at 214 nm, and fractions collected every 1 min. A total of 20 fractions were desalted with a Strata X C18 column and vacuum-dried.

2.5 LC-MS/MS analysis

Each fraction was resuspended in buffer A (5% ACN, 0.1% formic acid) at a final concentration of 0.5 μg/μL. Aliquots (10 μL) of supernatant were loaded on a LC-20AD nanoHPLC (Shimadzu, Japan) using the autosampler onto a 2 cm C18 trap column. Peptides were eluted onto a 10 cm analytical C18 column (inner diameter, 75 μm) packed in-house. Samples were loaded at 8 μL/min for 4 min and a 35 min gradient run at 300 nL/min, starting from 2 to 35% B (95% ACN, 0.1% FA), followed by a 5 min linear gradient to 60%, 2 min linear gradient to 80% and maintenance at 80% B for 4 min, returning to 5% in 1 min.

Data acquisition was performed with a TripleTOF 5600 System (AB SCIEX, Concord, ON) fitted with a Nanospray III source (AB SCIEX) and a pulled quartz tip as the emitter (New Objectives, Woburn, MA, USA). Data were acquired using an ion spray voltage of 2.5 kV, curtain gas of 30 psi, nebulizer gas of 15 psi, and an interface heater temperature of 150°C. The MS was operated with a RP of greater than or equal to 30 000 FWHM for TOF MS scans. For IDA, survey scans were acquired in 250 ms, and as many as 30 product ion scans collected if exceeding a threshold of 120 counts per

second (counts/s) and with a 2+ to 5+ charge state. The total cycle time was fixed to 3.3 s. The Q2 transmission window was 100 Da for 100%. Four time bins were summed for each scan at a pulser frequency value of 11 kHz through monitoring of the 40 GHz multichannel TDC detector with four-anode/channel detection. The sweeping collision energy was set to 35 ± 5 eV, and dynamic exclusion was set for 1/2 of peak width (15 s).

2.6 Data analysis

Acquired MS raw data files were converted into MGF files using Proteome Discoverer 1.2 (PD 1.2, Thermo), [5600 ms converter], and the MGF file searched. Proteins were identified using MASCOT search engine (Matrix Science, London, UK; version 2.3.02) against the Ensembl database (ftp://ftp.ensembl.org/pub/release-80/fasta/ovis_aries/pep/, Oar v3.1 version) containing 22730 sheep genome sequences [34]. For protein identification, mass tolerance of 0.05 Da (ppm) was permitted for intact peptide masses and 0.1 Da for fragmented ions, with allowance for one missed cleavage in the trypsin digests. Gln→pyro-Glu (N-term Q), Oxidation (M), Deamidated (NQ) were the potential variable modifications, and Carbamidomethyl (C), iTRAQ8plex (N-term), and iTRAQ8plex (K) were fixed modifications. The charge states of peptides were set to +2 and +3. Specifically, an automatic decoy database search was performed in MASCOT by choosing the decoy checkbox in which a random sequence of database is generated and tested for raw spectra as well as the real database. To reduce the probability of false peptide identification, only peptides at the 95% confidence interval (above the "identity" threshold) defined by MASCOT probability analysis were counted as identified. Each confident protein identification involved at least one unique peptide. For quantitation, a protein was required to contain at least two unique spectra. The quantitative protein ratios were weighted and normalized by the median ratio in MASCOT. We specifically used ratios with p-values < 0.05, and only fold changes >1.5 or <0.667 were considered significant.

2.7 Real-time RT-PCR

To verify the differentially expressed proteins identified using iTRAQ at the transcriptional level, ST cells infected with BTV-1 or mock-infected with culture medium were harvested at 24 and 48 hpi, and cellular total RNA extracted with TRIzol (Invitrogen, USA). After treatment with RNase-free DNase, 4 μg of each total RNA was reverse-transcribed with PrimerScript RT Enzyme Mix I, Oligo dT(18) primer and random primer (TaKaRa, Japan). Real-time PCR was performed on Mx3500p (Agilent Technologies, Germany) using a SYBR® Premix Ex Taq™ kit (TaKaRa, Japan) following the manufacturer's instructions. The primers used for amplifying cDNA of CASP8, DDX58, eIF4a1, HSP27, IFIH1, IFIT3, ISG20, OAS1, RSAD2, STAT1 and β-actin are presented in Table 1. Sheep β-actin was selected as the internal reference gene. Real-time RT-PCR for each gene was performed in triplicate. The relative expression level of each target gene in infected samples was calculated using $2^{-\Delta\Delta CT}$, representing n-fold change relative to the mock-infected sample [35].

2.8 Western blot analysis

Cell lysates of BTV-1-infected and mock-infected cultures were harvested at 24 and 48 hpi, and protein concentrations were determined. Equivalent amounts of cell lysates from the three replicates were denatured in 1×protein loading buffer by heating at 100°C for 5 min and separated via 12% SDS-PAGE. Protein bands in each gel were electrophoretically transferred onto PVDF membranes (Millipore, USA). Membranes were blocked with 5% fat-free milk and 0.5% Tween-20 in PBS for 1 h at room temperature, and incubated with rabbit polyclonal antibodies against HSP27, β-actin, STAT1, and eIF4a1 (Bioworld, USA) at 4°C overnight. After washing three times with PBS containing Tween-20, membranes were incubated with alkaline phosphatase-conjugated secondary antibodies (Sigma, USA) at room temperature for 1 h. Protein bands were detected using BCIP/NBT (Sigma, USA), and the intensity of the bands was measured using ImageJ software.

2.9 Bioinformatic analysis

The differentially expressed proteins identified in this study were converted to human orthologous proteins, and the lists submitted to the database for annotation, visualization, integrated discovery (DAVID) online server (http://david.abcc.ncifcrf.gov) and UniProt databases. Categories belonging to biological processes (GO-BP), molecular functions (GO-MF), and cellular components (GO-CC) identified at a confidence level of 95% were included in the analysis. The Kyoto Encyclopedia of Genes and Genomes (KEGG) pathway analysis was used to classify and group the identified proteins. The protein-protein interaction network was analyzed using the STRING 10 database (http://string.embl.de/).

3 Results

3.1 Confirmation of BTV replication in ST cells

To determine the morphology of ST cells and the optimal time-point for proteomic analysis following BTV infection, the growth kinetics of BTV replication in primary ST cells was determined by monitoring CPE and viral titers at 0, 12, 24, 48 and 72 hpi. Compared to mock-infected cells, CPE was minimal at 24 hpi and significant at 48 and 72 hpi, characterized by rounding, swelling, granular degeneration and

Table 1. Primer sequences used for real-time RT-PCR

Primer name	Sequence	Product size (bp)
CASP8 forward	5′-GCACTACAGAGACCAAACAGCAA-3′	142
CASP8 reverse	5′-TTGCCCATCAGAGCCATAGA-3′	
DDX58 forward	5′-CAGTGCAATCTGGTCATCCTCTAC-3′	84
DDX58 reverse	5′-CCCTCTTGCTCTTCCTCTACCTC-3′	
eIF4a1 forward	5′-CTTGTATGAAACCCTGACCATTACC-3′	82
eIF4a1 reverse	5′-CATCTTCTCGGTGAGCCAATC-3′	
HSP27 forward	5′-CGCCCTGGTGTGTAACTCTTGT-3′	234
HSP27 reverse	5′-GGAAGGTGACGGGAATGGT-3′	
IFIH1 forward	5′-GACCTCACGGACTTGCCTTC-3′	137
IFIH1 reverse	5′-AGTTTCTCCTCCACACATTTATCCA-3′	
IFIT3 forward	5′-CCATACCAAACAATGCCTACCTC-3′	168
IFIT3 reverse	5′-GCCCCTTCTCAATCGCTCT-3′	
ISG20 forward	5′-TGCTCTGCTCACCCCAACT-3′	121
ISG20 reverse	5′-CCGTTCCCCTTTTGCTCTC-3′	
OAS1 forward	5′-CTCAGGGATTTCGGACTGTTTT-3′	99
OAS1 reverse	5′-GGCTAATCGTAGGGTTTTCCAAG-3′	
STAT1 forward	5′-GGTGAAGTTGCAAGAGCTGA-3′	135
STAT1 reverse	5′-TCCATGTTCATCACCTTCGT-3′	
RSAD2 forward	5′-CATCCTCGCCATCTCCTGT-3′	80
RSAD2 reverse	5′-CGTGGTTCTTCTTTCCTTGACC-3′	
β-actin forward	5′-CTATGAGCTGCCCGATGGT-3′	122
β-actin reverse	5′-TGAAGGTGGTCTCGTGGATG-3′	

detachment of cells. At 72 hpi, almost all the cells had detached (Fig. 1A). The one-step growth curve revealed that viral titer reached 5.1×10^7 PFU/mL at 48 hpi, followed by a gradual decline (Fig. 1B). Generally, the time-point at which viral replication remains high with no significant host cell cytoskeleton or membrane rearrangement is taken as the optimal window for proteomic analysis. To ensure a higher percentage of infected cells and avoid excessive CPE, BTV- and mock-infected cells were harvested at 24 and 48 hpi for further proteomic analysis. Virus infection at different time-points

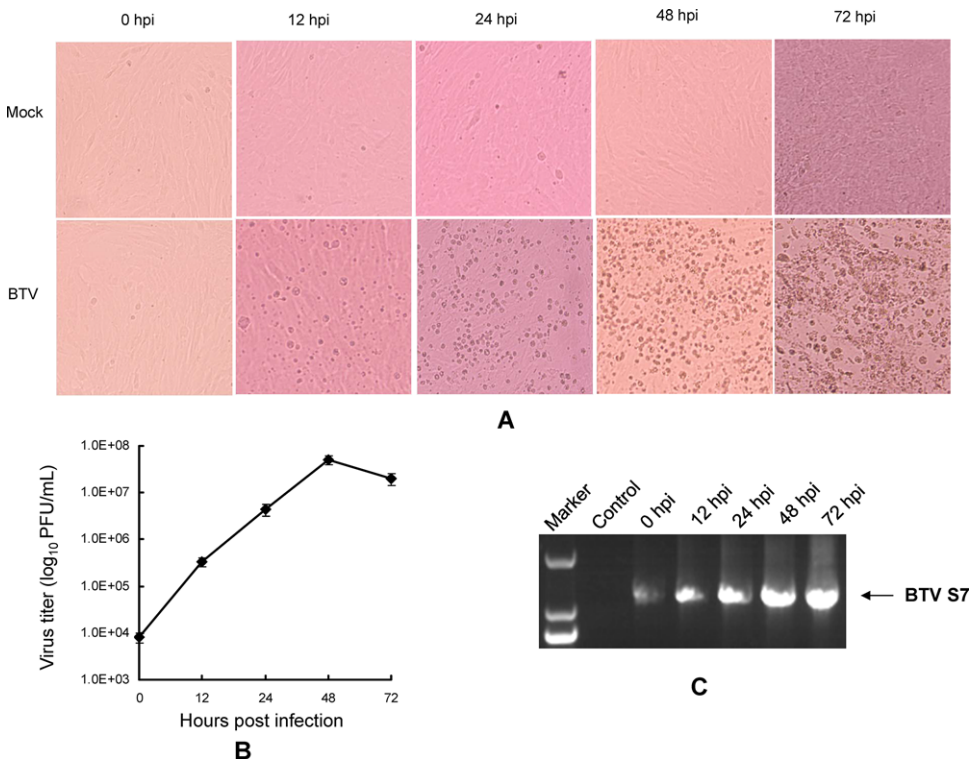

Figure 1. Confirmation of BTV infection in ST cells. (A) Morphological changes in ST cells at different time-points after BTV infection (MOI = 0.1), with mock-infected cells as a control. (B) Virus titers of BTV in ST cells expressed as PFU/mL on a logarithmic scale at different times post-infection. (C) RT-PCR validation of BTV infection in ST cells by amplifying the S7 gene.

Table 2. Differentially expressed proteins identified via iTRAQ analysis of ST cells infected with BTV-1

Accession number	Protein name	Gene symbol	Peptide	Coverage	Infected/uninfected (24 h) ratio	Infected/uninfected (48 h) ratio
Proteins showing increased abundance in BTV-infected cells						
ENSOARP00000015710	Radical S-adenosyl methionine domain-containing protein 2	RSAD2	7	20.7	16.39*	9.18*
ENSOARP00000011754	Interferon-stimulated gene 20 kDa protein	ISG20	2	11.7	10.53*	14.73*
ENSOARP00000008103	Protein VPRBP	VPRBP	1	0.5	7.35*	0.196
ENSOARP00000016273	Interferon-induced protein with tetratricopeptide repeats 2	IFIT2	8	18.6	6.25*	7.38*
ENSOARP00000015874	Interferon-induced protein with tetratricopeptide repeats 3	IFIT3	10	23.6	5.43*	5.38*
ENSOARP00000009432	Interferon beta-2	IFNB2	3	15.1	4.59*	3.09
ENSOARP00000011035	Interferon-induced GTP-binding protein Mx1	MX1	14	30.6	4.57*	9.06
ENSOARP00000010974	Interferon-induced GTP-binding protein Mx2	MX2	15	31.7	4.10*	6.07
ENSOARP00000019646	Vascular cell adhesion protein 1	VCAM1	9	15.2	3.97*	2.59
ENSOARP00000014407	Interferon-induced protein 44	IFI44	2	4.4	3.85*	7.46*
ENSOARP00000007752	Ubiquitin-like protein ISG15	ISG15	5	36.7	3.46*	5.07*
ENSOARP00000005319	C-C motif chemokine 5 (Fragment)	CCL5	1	9.9	3.44*	2.45
ENSOARP00000016282	Interferon-induced protein with tetratricopeptide repeats 1	IFIT1	10	25.1	3.25*	7.63
ENSOARP00000019807	Coagulation factor XIII A chain (Fragment)	F13A	2	3.8	3.22*	4.46
ENSOARP00000006578	Interferon-induced helicase C domain-containing protein 1	IFIH1	5	4.8	3.18*	6.89*
ENSOARP00000003061	2′-5′-oligoadenylate synthase 1	OAS1	2	13.0	3.02*	4.01*
ENSOARP00000001192	Probable E3 ubiquitin-protein ligase HERC6	HERC6	2	2.7	2.89*	4.97
ENSOARP00000002385	Indoleamine 2,3-dioxygenase 1	I23O1	3	8.3	2.79*	7.16*
ENSOARP00000010460	Interferon-induced, double-stranded RNA-activated protein kinase	E2AK2	8	15.7	2.72*	7.08*
ENSOARP00000020639	Proteasome activator complex subunit 2	PSME2	1	3.8	2.72*	2.05
ENSOARP00000018175	Caspase-8	CASP8	5	10.0	2.59*	4.23*
ENSOARP00000008124	Antigen peptide transporter 2	TAP2	13	23.5	2.58*	1.93*
ENSOARP00000008309	Antigen peptide transporter 1	TAP1	11	20.5	2.53*	2.94
ENSOARP00000006537	protein MB21D1	CGAS	3	11.7	2.43*	2.46*
ENSOARP00000001017	E3 ubiquitin-protein ligase RNF213	RN213	22	5.0	2.35*	2.99
ENSOARP00000002141	Tryptophan–tRNA ligase, cytoplasmic	SYWC	6	17.3	2.29*	3.22*
ENSOARP00000015803	Probable ATP-dependent RNA helicase DDX58	DDX58	10	12.8	2.19*	6.87*
ENSOARP00000005819	Protein NDRG1	NDRG1	2	7.7	2.18*	1.48
ENSOARP00000010079	Tapasin	TPSN	4	13.1	2.09*	2.00
ENSOARP00000016376	Plasminogen activator inhibitor 1	PAI1	9	23.9	2.07*	2.23
ENSOARP00000015890	Interferon-induced protein with tetratricopeptide repeats 5	IFIT5	2	3.7	2.07*	2.12
ENSOARP00000014916	Signal transducer and activator of transcription 1	STAT1	17	24.7	2.07*	3.26
ENSOARP00000004532	Protein PML	PML	10	13.5	2.04*	2.50*
ENSOARP00000014655	SCY1-like protein 2	SCYL2	2	2.9	1.98*	0.95

Table 2. Continued

Accession number	Protein name	Gene symbol	Peptide	Coverage	Infected/uninfected (24 h) ratio	Infected/uninfected (48 h) ratio
ENSOARP00000022614	Normal mucosa of esophagus-specific gene 1 protein	NMES1	4	48.2	1.94*	2.11*
ENSOARP00000017858	TPR and ankyrin repeat-containing protein 1	TRNK1	3	1.1	1.93*	3.97*
ENSOARP00000014741	Heat shock protein beta-1	HSP27	4	23.4	1.93*	2.47
ENSOARP00000009772	2′-5′-oligoadenylate synthase 2	OAS2	6	5.3	1.93*	3.33*
ENSOARP00000008552	Nuclear pore complex protein Nup160	NU160	5	4.1	1.90*	1.11
ENSOARP00000014392	Interferon-induced protein 44-like	IF44L	3	9.1	1.87*	2.28*
ENSOARP00000008165	Exportin-5	XPO5	3	2.6	1.85*	2.12*
ENSOARP00000006076	26S proteasome non-ATPase regulatory subunit 5	PSMD5	4	7.7	1.85*	1.67*
ENSOARP00000013906	Unconventionnal myosin-X	MYO10	6	3.1	1.81*	1.81*
ENSOARP00000011613	Rho GTPase-activating protein 35	RHG35	3	1.9	1.78*	2.36*
ENSOARP00000004472	Ubiquitin thioesterase OTUB1	OTUB1	6	27.6	1.75*	1.30
ENSOARP00000017007	Ubiquitin-conjugating enzyme E2 N	UBE2N	2	11.1	1.74*	0.98
ENSOARP00000021976	EH domain-containing protein 4	EHD4	8	20.0	1.72*	1.91*
ENSOARP00000013307	Opioid growth factor receptor	OGFR	3	8.4	1.72*	2.97
ENSOARP00000008882	Pyridoxal-dependent decarboxylase domain-containing protein 1	PDXD1	5	7.1	1.71*	1.93*
ENSOARP00000019117	Endoplasmic reticulum aminopeptidase 1	ERAP1	7	7.9	1.71*	1.12
ENSOARP00000002728	Activator of 90 kDa heat shock protein ATPase homolog 1	AHSA1	3	8.6	1.71*	1.19
ENSOARP00000004366	NEDD8 ultimate buster 1 (Fragment)	NUB1	4	9.1	1.70*	2.50
ENSOARP00000015129	ATPase family AAA domain-containing protein 1	ATAD1	5	14.4	1.70*	1.22
ENSOARP00000007946	Ribonuclease inhibitor	RINI	3	39.2	1.70*	1.42*
ENSOARP00000006493	LisH domain and HEAT repeat-containing protein KIAA1468	K1468	2	2.6	1.69*	1.48
ENSOARP00000018446	Dynamin-2	DYN2	6	11.8	1.68*	1.78*
ENSOARP00000018260	25-hydroxycholesterol 7-alpha-hydroxylase	CP7B1	3	5.5	1.68*	1.32
ENSOARP00000009260	Perilipin-3	PLIN3	5	16.5	1.68*	1.61*
ENSOARP00000001081	Developmentally-regulated GTP-binding protein 2	DRG2	3	11.5	1.67*	2.88*
ENSOARP00000001415	COMM domain-containing protein 3	COMD3	1	6.2	1.67*	1.33
ENSOARP00000019836	Heme oxygenase 1	HMOX1	5	24.0	1.64*	1.40*
ENSOARP00000017457	Negative elongation factor C/D	NELFD	3	5.3	1.63*	1.57*
ENSOARP00000000358	Nuclear pore complex protein Nup107	NU107	7	8.2	1.63*	1.71*
ENSOARP00000003137	Double-stranded RNA-specific adenosine deaminase	DSRAD	12	11.5	1.63*	2.54*
ENSOARP00000013662	Ataxin-3	ATX3	2	5.9	1.63*	2.09
ENSOARP00000003736	Tubulin-specific chaperone E	TBCE	3	6.4	1.63*	1.58*
ENSOARP00000019486	2′,3′-cyclic-nucleotide 3′-phosphodiesterase	CN37	6	12.8	1.61*	1.02
ENSOARP00000015534	Eukaryotic initiation factor 4A-I	eIF4A1	8	38.8	1.59*	2.84*
ENSOARP00000020612	Importin-4	IPO4	3	3.1	1.59*	2.58

Table 2. Continued

Accession number	Protein name	Gene symbol	Peptide	Coverage	Infected/uninfected (24 h) ratio	Infected/uninfected (48 h) ratio
ENSOARP00000016467	Importin subunit alpha-2	IMA2	7	16.4	1.58*	1.13
ENSOARP00000019059	Deubiquitinating protein VCIP135	VCIP1	3	3.6	1.57*	1.75*
ENSOARP00000010977	DBIRD complex subunit KIAA1967	K1967	9	14.2	1.56*	1.80
ENSOARP00000010473	Adapter protein CIKS	CIKS	2	3.7	1.56*	4.25
ENSOARP00000000590	E3 SUMO-protein ligase RanBP2 (Fragment)	RANBP2	12	4.7	1.56*	1.13
ENSOARP00000018654	Guanine nucleotide-binding protein G subunit alpha-1	GNAI1	1	19.0	1.56*	1.52*
ENSOARP00000005220	U3 small nucleolar RNA-associated protein 15 homolog	UTP15	4	8.3	1.55*	0.87
ENSOARP00000013891	Guanine nucleotide-binding protein-like 1	GNL1	2	3.1	1.54*	2.58*
ENSOARP00000013829	Hexokinase-2	HXK2	13	21.7	1.53*	1.96*
ENSOARP00000013594	Importin-7	IPO7	6	7.1	1.52*	1.68*
ENSOARP00000020750	Ubiquitin-like-conjugating enzyme ATG3	ATG3	3	11.5	1.52*	1.98
ENSOARP00000017974	Nucleoporin p54	NUP54	6	16.2	1.51*	1.41*
ENSOARP00000019761	Formin-like protein 3	FMNL3	10	10.8	1.51*	1.47*
ENSOARP00000022035	Macrophage-capping protein	CAPG	7	20.7	1.51*	1.32
Proteins showing decreased abundance in BTV-infected cells						
ENSOARP00000000336	Plexin domain-containing protein 2	PXDC2	3	4.7	0.66*	0.53
ENSOARP00000019983	Collagen alpha-1(XI) chain	COBA1	6	5.2	0.65*	0.47*
ENSOARP00000009036	39S ribosomal protein L14, mitochondrial	RM14	3	16.6	0.65*	0.63
ENSOARP00000007935	Fatty acyl-CoA reductase 1	FACR1	7	15.1	0.65*	0.47
ENSOARP00000005767	L-allo-threonine aldolase	LTAA	3	10.2	0.65*	0.70
ENSOARP00000013281	C-type mannose receptor 2	MRC2	2	1.8	0.65*	0.54
ENSOARP00000005693	Drebrin	DREB	9	19.9	0.63*	0.54*
ENSOARP00000015742	Acyl-CoA desaturase	ACOD	1	2.7	0.62*	0.38
ENSOARP00000001046	Alpha-2-macroglobulin	A2MG	13	10.8	0.58*	1.04
ENSOARP00000019765	Peptidyl-glycine alpha-amidating monooxygenase	AMD	5	6.2	0.57*	0.66*
ENSOARP00000004450	Immunoglobulin superfamily containing leucine-rich repeat protein 2	ISLR2	4	6.7	0.51*	0.26*
ENSOARP00000015287	Connective tissue growth factor	CTGF	5	17.3	0.48*	0.46*
ENSOARP00000022056	Alpha-2-HS-glycoprotein	FETUA	2	4.0	0.40*	1.09
ENSOARP00000018386	Keratin, type II microfibrillar (Fragment)	K2M1	2	6.3	0.39*	1.29
ENSOARP00000004100	Alpha-1B-glycoprotein	A1BG	3	5.9	0.30*	1.11
ENSOARP00000009080	Serotransferrin	TRFE	12	16.2	0.28*	0.98
ENSOARP00000015963	Alpha-1-antiproteinase	A1AT	2	4.8	0.23*	0.96
ENSOARP00000015112	Alpha-2-antiplasmin	A2AP	1	1.6	0.22*	1.74

*Represents significant difference (p-value<0.05).

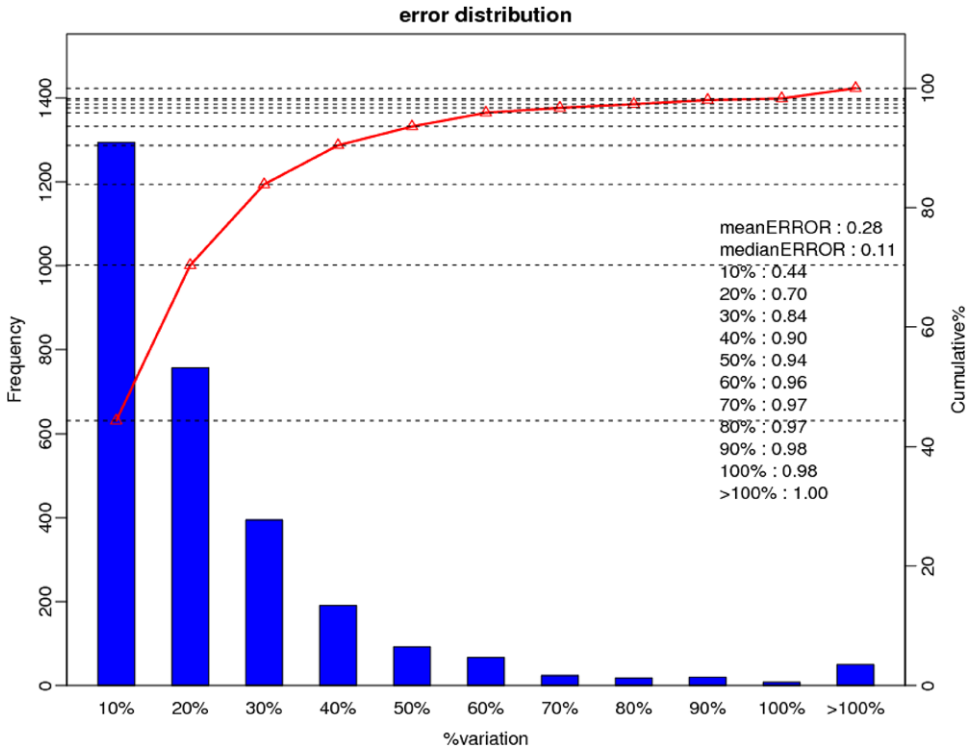

Figure 2. Correlation of uninfected ST cells between the two time-points (24 and 48 hpi). The x-axis represents the variation levels of proteins in uninfected ST cells between the two time-points. The left y-axis represents the frequency of quantitative proteins (histograms) and the right y-axis represents the cumulative percentage of proteins at different variation levels (line graph).

was additionally confirmed via RT-PCR using a total of 23 cycles. Abundance of viral S7 RNAs increased gradually over time until 48 hpi (Fig. 1C). Sequencing analysis of PCR products further validated BTV infection (data not shown).

3.2 Identification of differentially expressed proteins

The host response to BTV-1 infection at 24 and 48 hpi was analyzed by examining differences in protein expression. To identify the proteins differentially expressed between BTV-infected and mock-infected ST cells, we conducted iTRAQ-based quantitative proteomic analyses. iTRAQ-labeled samples were subsequently analyzed via LC−MS/MS. Using this approach, a total of 17 471 peptides and 4455 proteins were detected and quantified, among which 101 and 479 proteins displayed significant differences in expression between BTV- and mock-infected cells at 24 and 48 hpi, respectively, identified by at least two high confidence score (95%) peptides with p-values <0.05, calculated using ProQUANT. At 24 hpi, 83 and 18 proteins were significantly up- and down-regulated (Table 2), while 345 and 134 proteins were significantly up- and down-regulated, respectively, at 48 hpi (Supporting Information Table S1), according to the criteria (p-values < 0.05, and fold changes >1.5 or <0.667). Furthermore, 48 proteins (43 upregulated and five downregulated) were significantly dysregulated between the two time-points. We observed a greater number of significantly expressed immune-related proteins at 24 than 48 hpi. In view of the growing research interest on antiviral proteins, here we focused on proteins that were differentially expressed during the earlier stages of infection. Figure 2 depicts the correlation of uninfected ST cells between the two time-points (24 and 48 hpi). Proteins showing lower than 50% variation accounted for 94% of the total proteins, indicating significant correlation. Since the current sheep genome database is poorly annotated compared to the human genome database, 55 proteins remained unassigned or uncharacterized, resulting in a large number of predicted proteins in our analysis. Further research focusing on the functions of these proteins is therefore warranted.

3.3 Validation of differentially expressed proteins

To validate the differentially expressed proteins identified via iTRAQ-labeled LC-MS/MS analysis, transcriptional profiles of ten selected cellular proteins of ST cells with and without BTV infection were analyzed at 24 and 48 hpi. Real-time RT-PCR results showed that the at 24 hpi, mRNA levels of CASP8, DDX58 (also known as RIG-I), eIF4a1, HSP27, IFIH1 (also known as MDA5), IFIT3, ISG20, OAS1, RSAD2 (also known as viperin), and STAT1 were increased by 3.44-, 3.45-, 2.72-, 1.83-, 2.53-, 4.06-, 5.12-, 2.03-, 9.06-, and 1.67-fold, respectively, and by 3.03-, 6.36-,3.16-,4.03-, 7.02-, 3.80-, 4.23-, 2.91-, 10.67- and 2.33-fold, respectively, at 48 hpi (Fig. 3A), consistent with iTRAQ labeled LC–MS/MS data. For further confirmation of proteomic data, three of the proteins, eIF4a1, STAT1 and HSP27, were selected for western blot analysis. As

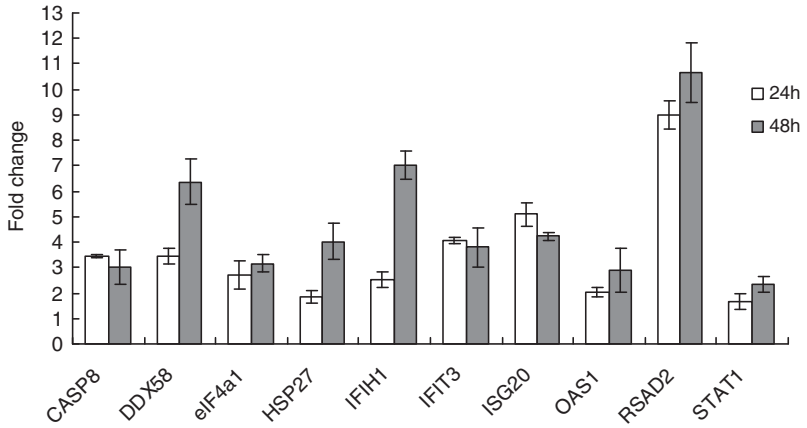

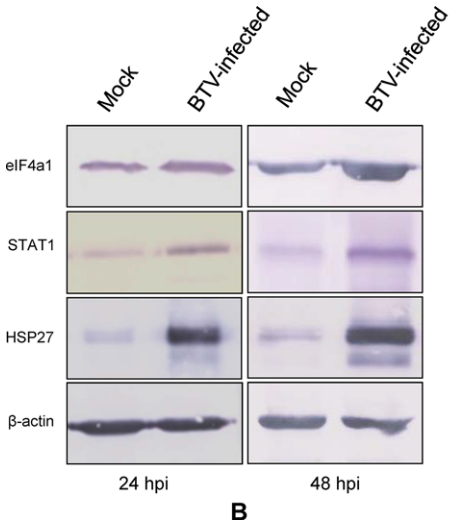

	WB ratio		iTRAQ ratio	
	24hpi	48 hpi	24hpi	48 hpi
eIF4a1	1.58	2.11	1.59	2.84
STAT1	2.66	2.92	2.07	3.26
HSP27	5.31	5.92	1.93	2.47

C

Figure 3. Confirmation of differentially expressed proteins with real-time RT-PCR or western blot. (A) Real-time RT-PCR analysis of ten selected genes in BTV-infected cells and control samples. ST cells were infected with BTV or mock-infected at MOI of 0.1, and collected at 24 and 48 hpi. Total RNA was extracted and reverse-transcribed into cDNA for subsequent analysis via quantitative PCR. Fold-change values were calculated according to the $2^{-\Delta\Delta CT}$ method, using β-actin as an internal reference. Error bars represent the standard error of three independent experiments. (B) Western blot analysis of β-actin, STAT1, eIF4a, and HSP27 in BTV-infected and control samples at 24 and 48 hpi. Equal amounts of protein from BTV and mock-infected cells were separated using SDS-PAGE and transferred to PVDF membranes. The membranes were probed with the appropriate antibodies, and bands visualized. β-actin was used as the internal reference. The images shown are representatives of three independent experiments. (C) The intensity ratio between the corresponding bands (BTV-infected band/Mock band) was determined using ImageJ and normalized against β-actin .

shown in Fig. 3B, the three representative proteins were up-regulated in BTV-infected ST cells at 24 and 48 hpi, in keeping with the alterations in protein expression during BTV infection identified using iTRAQ analysis (Fig. 3C).

3.4 Functional classification of the identified proteins

To annotate the potential biological functions of the 101 differentially regulated proteins upon BTV infection, proteins were analyzed via gene ontology (GO) enrichment using the online DAVID and UniProt databases. Three major annotation types were obtained from the GO consortium website: cellular components, molecular functions, and biological processes. The cellular component annotation (GO-CC) revealed that the differentially expressed proteins were well distributed within different cell components, with intrinsic to membrane and organelle lumen being two highly distributed components (12 and 11 proteins, respectively) (Fig. 4A). The molecular function (GO-MF) annotation demonstrated that proteins related to cation binding, nucleotide binding and enzyme binding were most commonly affected by viral infection (Fig. 4B). The biological process (GO-BP) annotation revealed that differentially regulated proteins are involved in nucleocytoplasmic transport, immune response, signal transduction, transcription, apoptosis, stress response, and antigen processing and presentation (Fig. 4C). To further investigate the pathway involvement of these proteins, KEGG pathway analysis based on the DAVID program was performed. Although most of the grouped pathways of the KEGG analysis were not statistically significant, these data sorted and grouped differentially expressed proteins based on function. According to the results, differentially expressed proteins were mainly involved in the RIG-I-like receptor signaling pathway and endocytosis (Fig. 4D).

3.5 Analysis of protein-protein interactions

To clarify the mechanisms underlying BTV interactions with proteins of ST cells and consequent effects on cell function,

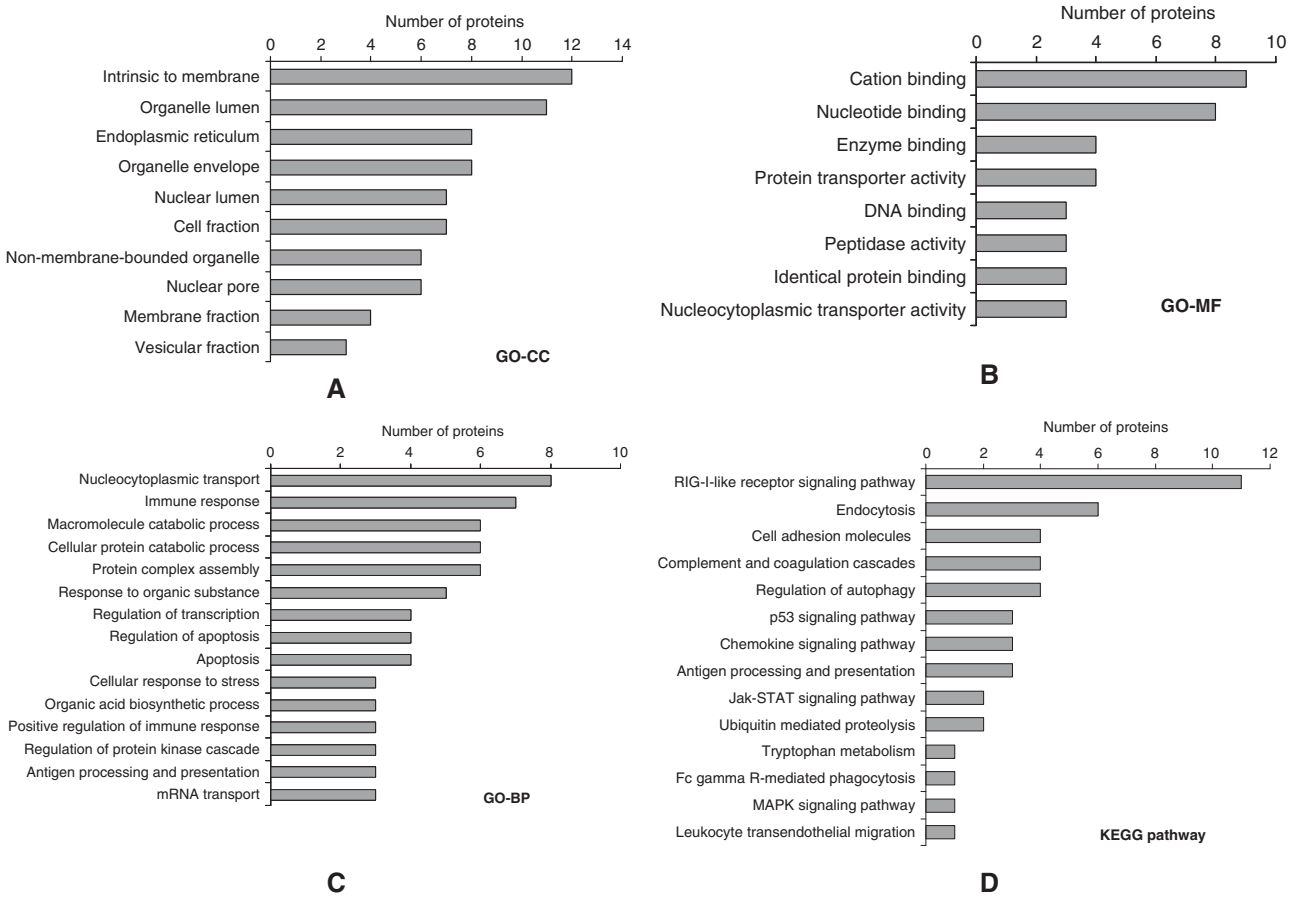

Figure 4. GO and KEGG pathway enrichment analysis of 101 differentially expressed proteins based on their functional annotations. (A) Analysis of cellular component (GO-CC); (B) analysis of molecular function (GO-MF); (C) analysis of biological process (GO-BP); (D) KEGG Pathway enrichment analysis.

101 differentially expressed proteins were further analyzed by searching the STRING database and protein–protein interaction networks. As demonstrated in Fig. 5, we identified two groups of strongly interacting proteins that were significantly regulated by BTV, including the ISG family regulated by IFN, STAT1-ISG15-ISG20-OAS1-OAS2-Mx1-Mx2-DDX58-IFIT1-IFIT2-IFIT3-IFIT5-IFI44-IFIH1-ADAR-RSAD2-HERC6-PML, and nuclear pore complex (NPC) proteins, RanBP2-Nup5-IPO4-IPO7-XPO5. These seed proteins have important functions in innate immune response and nuclear pore transport. For instance, IFIH1 (MDA5) is an innate immune receptor that acts as a cytoplasmic sensor of viral nucleic acids with a major role in sensing viral infection and activation of a cascade of antiviral responses, including induction of type I interferons and proinflammatory cytokines [36]. RanBP2 (originally named Nup358) is a large cyclophilin-related nuclear pore protein involved in the Ran-GTPase cycle that orchestrates the majority of nuclear import and export and also required for nuclear import or viral DNA integration of human immunodeficiency virus [37]. These findings suggest that entirely different sets of host proteins, interactions and processes, including the immune response, are perturbed during BTV infection. The interaction networks that appear to be regulated by BTV should provide clues for further clarification of the impact of viral infection on the physiological functions of target cells and host response.

4 Discussion

Virus-cell interactions are highly complex, and gene expression, signaling and immune response pathways are commonly altered during viral infection [17, 18]. To date, no research has focused on differential proteome analysis of host cells in response to BTV infection. In the present study, iTRAQ coupled with LC-MS/MS was applied to analyze the differential proteome of ST cells infected with BTV. We obtained relative quantitative information for 4455 proteins in BTV- and mock-infected ST cells. At 24 hpi, the expression patterns of 101 (83 upregulated and 18 downregulated)

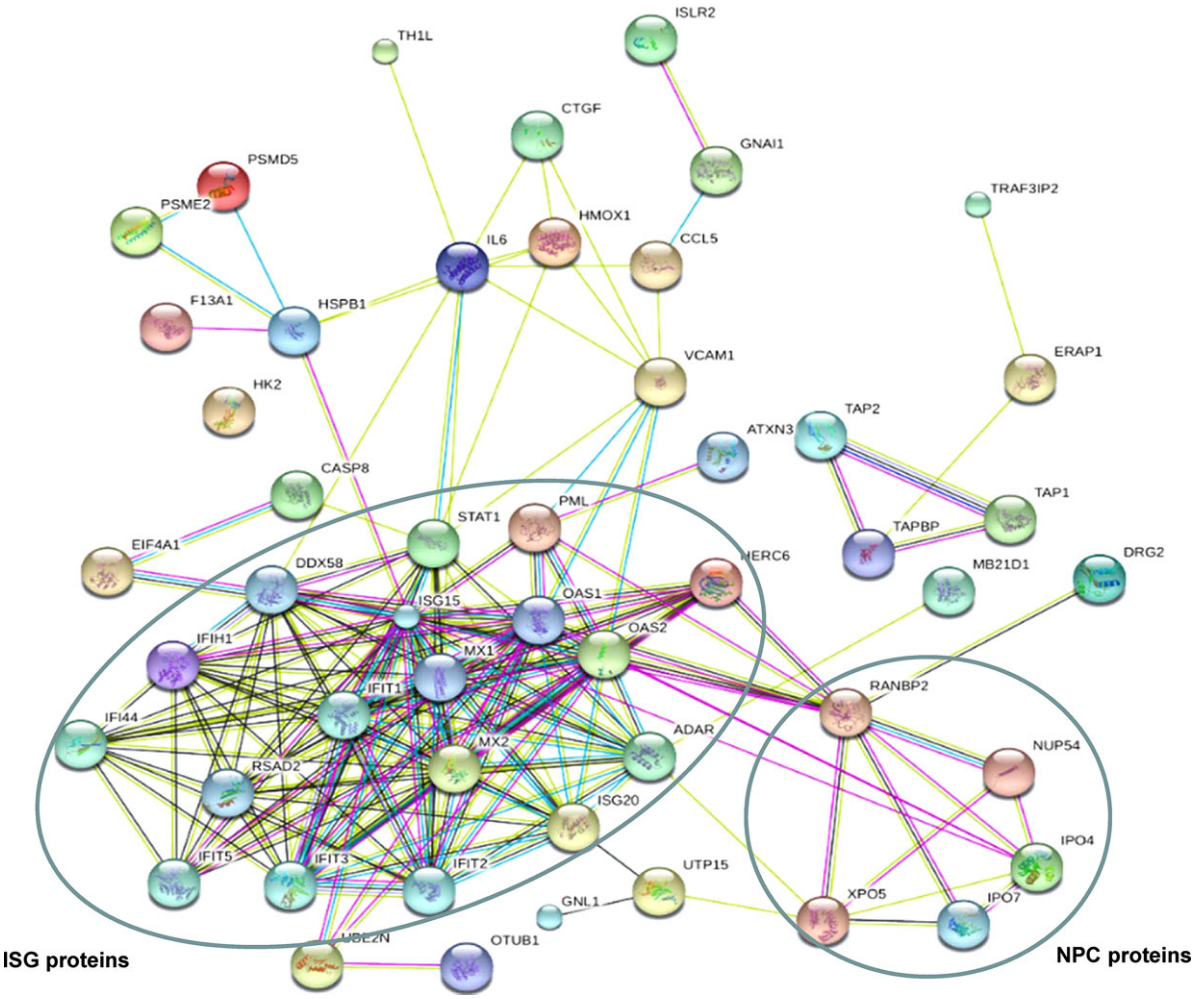

Figure 5. Interaction network of differentially expressed proteins generated using the STRING database. Network analysis was set at medium confidence (STRING score = 0.4). The edges represent predicted functional associations. An edge was drawn with up to seven different colored lines representing the existence of seven types of evidence used in predicting the associations. The red line indicates the presence of fusion evidence, the green line neighborhood evidence, the blue line co-occurrence evidence, the purple line experimental evidence, the yellow line textmining evidence, the light-blue line database evidence, and the black line co-expression evidence.

different host proteins were significantly changed while 479 proteins (345 upregulated and 134 downregulated) displayed significant alterations in expression at 48 hpi in BTV-infected cells, relative to mock-infected cells. Our data revealed a larger proteomic shift at 48 hpi, compared with 24 hpi, in BTV-infected ST cells. However, a greater number of innate immune proteins were differentially expressed at 24 than 48 hpi, and we identified numerous proteins related to the cell cycle, ribosome and chromosome maintenance at 48 hpi, indicating that cell morphological changes at the later stages of infection initiate the mechanism of cell maintenance. With antiviral response in mind, we focused on the differentially expressed proteins during the early stage of infection (24 hpi). Differential expression of three representative proteins, eIF4a1, STAT1 and HSP27, was validated via western blot. Since no specific antibodies against ovine CASP8, DDX58, IFIH1, IFIT3, ISG20, OAS1, and RSAD2 are available and no cross-reaction was detected with antibodies against the homologous human proteins (data not shown), real-time RT-PCR was used to analyze expression patterns of the ten selected proteins. Our data provide a comprehensive insight into the cellular response to BTV infection and the mechanisms involved in viral pathogenesis.

Since BTV infection usually causes severe symptoms in sheep, sheep primary testis cells were used to investigate the host response during BTV infection. Prior to proteomic analysis, we determined which time-points to investigate following infection by observing morphological changes and analyzing viral growth dynamics in BTV-infected cells. The results indicate that BTV induces CPE from 24 to 72 hpi in infected cells, compared to mock-infected cells. Production of mature particles was exponential at 8 and 24 h post-infection

[38]. Furthermore, virus titer was continuously increased in infected cells until 48 h, at which time we observed the highest viral load. At 72 hpi, all infected cells showed rounding and granular degeneration. BTV infection can terminate host protein expression in the late stage. Thus, to avoid detecting changes in host protein expression caused by interference with translation, proteomic analyses were performed on cells at early infection time-points (24 and 48 hpi). Some viruses, if passaged at MOI>1, accumulate spontaneously deleted defective particles that are maintained during passage by the presence of complementing wild-type helper virus [39]. For proteome profiling, although most cells could be infected under high MOI (such as MOI of 1), the levels of most host proteins would be nonspecifically reduced by translational repression or strongly affected by BTV-induced apoptosis. To avoid the changes in protein expression profiles masked by BTV-induced translational shutoff and apoptotic effects, ST cells were infected with BTV at a MOI of 0.1, rather than higher MOI. Therefore, in this study, we examined differentially expressed proteins regulated by BTV infection at MOI of 0.1 at 24 and 48 hpi.

The innate immune response is the first line of defence against viruses, involving production of type I IFN (IFN-α/β) and other pro-inflammatory cytokines that control infection. It also shapes the adaptive immune response generated by both T and B cells. Production of IFN in response to virus infection is triggered by the recognition of pathogen-associated molecular patterns by the infected cell. Activation of innate cellular responses during viral infection requires recognition of pathogen-associated molecular patterns by pattern recognition receptors [36,40,41]. The genome of BTV, composed of dsRNA molecules, has been described as a potent inducer of type I IFN, both in vivo and in vitro. Recent studies have shown that BTV triggers type I IFN production in plasmacytoid dendritic cells via a MYD88-dependent/TLR7/8-independent sensing and signaling pathway whereas cytoplasmic helicases (RIG-1, MDA5) mediate sensing and signaling in BTV-infected epithelial cells [42, 43]. However, pattern recognition receptor signaling pathways and the mechanisms responsible for production of IFN in response to BTV are still not completely understood. Type I IFN binds to a common IFN-α/β receptor (IFNAR), initiating a signaling cascade that results in expression of hundreds of interferon-stimulated genes (ISG). ISGs are key components of the host innate immune response and serve as the first line of defense against viral infection. In our study, 18 upregulated ISG proteins were identified. Among these, interferon-inducible ISG15, ISG20, Mx1, Mx2, RSAD2, OAS1 and OAS2, have been documented as critical antiviral proteins in cells and animals [44, 45]. IFIT proteins have also been shown to inhibit virus replication by binding and regulating the functions of cellular and viral proteins and RNAs [46]. DDX58 (RIG-1) plays an important role in the recognition of RNA viruses in various cells, and has been identified as a candidate cytoplasmic viral dsRNA receptor [47]. In the current study, we demonstrated that BTV infection induces overexpression of a number of antiviral proteins, several of which were identified for the first time, including ISG15, ISG20, Mx1, Mx2, RSAD2, OAS1, OAS2, IFI44 and IFIT [36, 48].

We additionally confirmed upregulation of STAT1, HSP27 and eIF4a1 via qRT-PCR and western blot analyses. Enhanced expression of STAT1, a key regulator of interferon-responsive genes [49], during BTV infection suggests that the virus activates canonical interferon signaling through the JAK-STAT1 pathway. HSP, also known as stress proteins, are often involved in antigen presentation and intracellular trafficking and apoptosis, and act as molecular chaperones by helping nascent polypeptides assume their proper conformations. HSP27 is linked to different signaling pathways that regulate cellular functions, such as inflammation, apoptosis, development, differentiation and cell growth. In addition, many other viruses, including avian influenza H9N2 [50], infectious bursal disease virus [21], and African swine fever virus [51], induce upregulation of HSP27. eIF4A1 was initially characterized based on its requirement in translation and later identified as a component of the eIF4F translation initiation complex responsible for RNA helicase activity [52]. Among the virus–host interactions, those that recruit cellular translational machinery to viral mRNAs play a decisive role in viral replication. Viral RNAs have evolved structures to maximize their translation and efficiently compete with cellular mRNAs [53, 54]. The issue of whether upregulation of eIF4A1 expression in BTV-infected ST cells is a contributory step in virus replication will be investigated in future studies.

The ubiquitin-proteasome system (UPS), a major intracellular degradation pathway for foreign proteins, plays a critical role in a variety of cellular functions, such as antigen processing, cell cycle regulation, apoptosis, signal transduction, transcriptional regulation, and DNA repair. Ubiquitination is a crucial cellular event in pathways for type I IFN activation [55, 56]. In addition to activation, signaling molecules in these pathways may be ubiquitinated for proteasomal degradation, consequently downregulating the IFN response. Viruses have evolved different strategies to utilize the UPS to their advantage. For example, activation of the UPS pathway is necessary for hepatitis E virus replication [57], and also required by other viruses, such as influenza virus [58], vaccinia virus [59], porcine reproductive and respiratory syndrome virus [60] and rotavirus [61]. In our study, nine UPS proteins, including HERC-6, UBE2N, ISG15, VPRBP, OTUB1, NUB1, RANBP2, PSMD5, and PSME2, were differentially upregulated at 24 hpi, indicating a relatively significant influence of the virus on the UPS pathway. The finding that the cellular UPS pathway is disrupted upon BTV infection supports the potential utility of an anti-UPS-based strategy in preventing infection. However, the particular UPS pathway employed by BTV to evade host immune surveillance remains to be established.

NPCs are embedded in pores of the nuclear envelope and constitute large aqueous transport channels that mediate and regulate the bidirectional exchange of macromolecules between the nucleus and cytoplasm [37, 62]. Our iTRAQ analysis for BTV-infected ST cells revealed that many

proteins involved in intracellular protein transport are significantly upregulated during BTV infection, including components of the NPC, such as RanBP2, Nup54, IPO4, IPO7 and XPO5, suggesting that infection by BTV enhances molecular transport between the nucleolus and cytoplasm and biological functions are possibly activated in the latter. Previous studies disclosed that NS4 of BTV starts to accumulate and shuttle between the nucleolus and cytoplasm as early as 4 hours post-infection and possibly interacts with the IFN pathway [6, 7]. Further research is needed to determine whether the upregulation of nuclear pore proteins is associated with trafficking of NS4 between the nucleolus and cytoplasm.

Apoptosis of host cells plays a major role in regulating the pathogenesis of many infectious diseases. Apoptosis triggered by virus infection directly leads to viral pathogenesis. However, blocking apoptosis can avoid premature death of infected cells, permitting a high titer of virus replication or persistent infection [63]. In our analysis, four apoptosis-related genes (Casp8, K1967, PML and CIKS) were identified following BTV infection. Caspase-8 is an initiator caspase activated by interactions between external apoptotic elements and cell surface molecules. BTV infection led to significant upregulation of caspase-8 in virus-infected ST cells, as verified with qRT-PCR. Regulation of cell death is known to be important for replication and pathogenesis in various Orbiviruses [64–66], and therefore, we propose that further investigation of these proteins should facilitate clarification of the mechanisms underlying cell death regulation during BTV infection.

In conclusion, the current study has provided a global overview of the protein alterations in BTV-infected ST cells. The identification of significantly altered proteins in BTV-infected ST cells reflects a comprehensive BTV-host cell interaction network. To our knowledge, many of the immune response-related proteins differentially expressed upon BTV infection are novel and have not been detected in previous studies [36, 48], thus providing new protein targets for evaluation in the future. Elucidation of the functions of these proteins in virus–host cell interactions may additionally uncover new therapeutic strategies targeting BTV.

This study was financially supported by ASTIP, Fundamental Research Incremental Program (2014ZL010), CAAS; China-South Africa Joint Research Projects (CS08-L13); Gansu International Collaboration Special Project (1504WKCA056); Scientific Research Foundation for the Returned Overseas Chinese Scholars, MOE (2015); NBCIS (CARS-38); Special Fund for Agro-scientific Research in the Public Research (No201303035), MOA; Jiangsu Co-innovation Center programme for Prevention and Control of Important Animal Infectious Diseases and Zoonoses; State Key Laboratory of Veterinary Etiological Biology Project.

The authors have declared no conflict of interest.

5 References

[1] Mellor, P. S., Boorman, J., The transmission and geographical spread of African horse sickness and bluetongue viruses. *Ann. Trop. Med. Parasitol.* 1995, *89*, 1–15.

[2] Maclachlan, N. J., Drew, C. P., Darpel, K. E., Worwa, G., The pathology and pathogenesis of bluetongue. *J. Comp. Pathol.* 2009, *141*, 1–16.

[3] Maan, N. S., Maan, S., Belaganahalli, M. N., Ostlund, E. N. et al., Identification and differentiation of the twenty six bluetongue virus serotypes by RT-PCR amplification of the serotype-specific genome segment 2. *PLoS One* 2012, *7*, e32601.

[4] OIE, *Manual of Diagnostic Tests and Vaccines for Terrestrial Animals*, 7th Edition, Paris 2012.

[5] Roy, P., Functional mapping of bluetongue virus proteins and their interactions with host proteins during virus replication. *Cell Biochem. Biophys.* 2008, *50*, 143–157.

[6] Ratinier, M., Caporale, M., Golder, M., Franzoni, G. et al., Identification and characterization of a novel non-structural protein of bluetongue virus. *PLoS Pathog.* 2011, *7*, e1002477.

[7] Belhouchet, M., Mohd Jaafar, F., Firth, A. E., Grimes, J. M. et al., Detection of a fourth orbivirus non-structural protein. *PLoS One* 2011, *6*, e25697.

[8] Jenckel, M., Breard, E., Schulz, C., Sailleau, C. et al., Complete coding genome sequence of putative novel bluetongue virus serotype 27. *Genome Announc.* 2015, *3*, e0016-15.

[9] Moulin, V., Noordegraaf, C. V., Makoschey, B., van der Sluijs, M. et al., Clinical disease in sheep caused by bluetongue virus serotype 8, and prevention by an inactivated vaccine. *Vaccine* 2012, *30*, 2228–2235.

[10] Gowen, B. B., Holbrook, M. R., Animal models of highly pathogenic RNA viral infections: hemorrhagic fever viruses. *Antiviral Res.* 2008, *78*, 79–90.

[11] Maan, S., Maan, N. S., Ross-smith, N., Batten, C. A. et al., Sequence analysis of bluetongue virus serotype 8 from the Netherlands 2006 and comparison to other European strains. *Virology* 2008, *377*, 308–318.

[12] Calvo-Pinilla, E., Castillo-Olivares, J., Jabbar, T., Ortego, J. et al., Recombinant vaccines against bluetongue virus. *Virus Res.* 2014, *182*, 78–86.

[13] Coetzee, P., Van Vuuren, M., Stokstad, M., Myrmel, M. et al., Viral replication kinetics and in vitro cytopathogenicity of parental and reassortant strains of bluetongue virus serotype 1, 6 and 8. *Vet. Microbiol.* 2014, *171*, 53–65.

[14] Elbers, A. R., Backx, A., Ekker, H. M., van der Spek, A. N., van Rijn, P. A., Performance of clinical signs to detect bluetongue virus serotype 8 outbreaks in cattle and sheep during the 2006-epidemic in The Netherlands. *Vet. Microbiol.* 2008, *129*, 156–162.

[15] Patel, A., Roy, P., The molecular biology of Bluetongue virus replication. *Virus Res.* 2014, *182*, 5–20.

[16] Du, J., Bhattacharya, B., Ward, T. H., Roy, P., Trafficking of bluetongue virus visualized by recovery of tetracysteine-tagged virion particles. *J. Virol.* 2014, *88*, 12656–12668.

[17] Friedel, C. C., Haas, J., Virus-host interactomes and global models of virus-infected cells. *Trends Microbiol.* 2011, *19*, 501–508.

[18] de Chassey, B., Meyniel-Schicklin, L., Aublin-Gex, A., Andre, P., Lotteau, V., New horizons for antiviral drug discovery from virus-host protein interaction networks. *Curr. Opin. Virol.* 2012, *2*, 606–613.

[19] Komarova, A. V., Combredet, C., Meyniel-Schicklin, L., Chapelle, M. et al., Proteomic analysis of virus-host interactions in an infectious context using recombinant viruses. *Mol. Cell. Proteomics* 2011, *10*, M110 007443.

[20] Sun, J., Jiang, Y., Shi, Z., Yan, Y. et al., Proteomic alteration of PK-15 cells after infection by classical swine fever virus. *J. Proteome Res.* 2008, *7*, 5263–5269.

[21] Zheng, X., Hong, L., Shi, L., Guo, J. et al., Proteomics analysis of host cells infected with infectious bursal disease virus. *Mol. Cell. Proteomics* 2008, *7*, 612–625.

[22] Chen, J. H., Chang, Y. W., Yao, C. W., Chiueh, T. S. et al., Plasma proteome of severe acute respiratory syndrome analyzed by two-dimensional gel electrophoresis and mass spectrometry. *Proc. Natl. Acad. Sci. U. S. A.* 2004, *101*, 17039–17044.

[23] Zhang, X., Zhou, J., Wu, Y., Zheng, X. et al., Differential proteome analysis of host cells infected with porcine circovirus type 2. *J. Proteome Res.* 2009, *8*, 5111–5119.

[24] Fan, H., Ye, Y., Luo, Y., Tong, T. et al., Quantitative proteomics using stable isotope labeling with amino acids in cell culture reveals protein and pathway regulation in porcine circovirus type 2 infected PK-15 cells. *J. Proteome Res.* 2012, *11*, 995–1008.

[25] Emmott, E., Wise, H., Loucaides, E. M., Matthews, D. A. et al., Quantitative proteomics using SILAC coupled to LC-MS/MS reveals changes in the nucleolar proteome in influenza A virus-infected cells. *J. Proteome Res.* 2010, *9*, 5335–5345.

[26] Emmott, E., Rodgers, M. A., Macdonald, A., McCrory, S. et al., Quantitative proteomics using stable isotope labeling with amino acids in cell culture reveals changes in the cytoplasmic, nuclear, and nucleolar proteomes in Vero cells infected with the coronavirus infectious bronchitis virus. *Mol. Cell. Proteomics* 2010, *9*, 1920–1936.

[27] Zhang, L. K., Chai, F., Li, H. Y., Xiao, G., Guo, L., Identification of host proteins involved in Japanese encephalitis virus infection by quantitative proteomics analysis. *J. Proteome Res.* 2013, *12*, 2666–2678.

[28] Pathak, S., De Souza, G. A., Salte, T., Wiker, H. G., Asjo, B., HIV induces both a down-regulation of IRAK-4 that impairs TLR signalling and an up-regulation of the antibiotic peptide dermcidin in monocytic cells. *Scand. J. Immunol.* 2009, *70*, 264–276.

[29] An, K., Fang, L., Luo, R., Wang, D. et al., Quantitative proteomic analysis reveals that transmissible gastroenteritis virus activates the JAK-STAT1 signaling pathway. *J. Proteome Res.* 2014, *13*, 5376–5390.

[30] Lu, Q., Bai, J., Zhang, L., Liu, J. et al., Two-dimensional liquid chromatography-tandem mass spectrometry coupled with isobaric tags for relative and absolute quantification (iTRAQ) labeling approach revealed first proteome profiles of pulmonary alveolar macrophages infected with porcine reproductive and respiratory syndrome virus. *J. Proteome Res.* 2012, *11*, 2890–2903.

[31] Liu, J., Bai, J., Lu, Q., Zhang, L. et al., Two-dimensional liquid chromatography-tandem mass spectrometry coupled with isobaric tags for relative and absolute quantification (iTRAQ) labeling approach revealed first proteome profiles of pulmonary alveolar macrophages infected with porcine circovirus type 2. *J. Proteomics* 2013, *79*, 72–86.

[32] Zeng, S., Zhang, H., Ding, Z., Luo, R. et al., Proteome analysis of porcine epidemic diarrhea virus (PEDV)-infected Vero cells. *Proteomics* 2015, *15*, 1819–1828.

[33] Du, C., Liu, H. F., Lin, Y. Z., Wang, X. F. et al., Proteomic alteration of equine monocyte-derived macrophages infected with equine infectious anemia virus. *Proteomics* 2015, *15*, 1843–1858.

[34] Jiang, Y., Xie, M., Chen, W., Talbot, R. et al., The sheep genome illuminates biology of the rumen and lipid metabolism. *Science* 2014, *344*, 1168–1173.

[35] Schmittgen, T. D., Livak, K. J., Analyzing real-time PCR data by the comparative C(T) method. *Nat. Protoc.* 2008, *3*, 1101–1108.

[36] Vitour, D., Doceul, V., Ruscanu, S., Chauveau, E. et al., Induction and control of the type I interferon pathway by Bluetongue virus. *Virus Res.* 2014, *182*, 59–70.

[37] Konig, R., Zhou, Y., Elleder, D., Diamond, T. L. et al., Global analysis of host-pathogen interactions that regulate early-stage HIV-1 replication. *Cell* 2008, *135*, 49–60.

[38] Schwartz-Cornil, I., Mertens, P. P., Contreras, V., Hemati, B. et al., Bluetongue virus: virology, pathogenesis and immunity. *Vet. Res.* 2008, *39*, 46.

[39] Von Magnus, P., Incomplete forms of influenza virus. *Adv. Virus Res.* 1954, *2*, 59–79.

[40] Akira, S., Uematsu, S., Takeuchi, O., Pathogen recognition and innate immunity. *Cell* 2006, *124*, 783–801.

[41] Yoneyama, M., Fujita, T., RNA recognition and signal transduction by RIG-I-like receptors. *Immunol. Rev.* 2009, *227*, 54–65.

[42] Chauveau, E., Doceul, V., Lara, E., Breard, E. et al., NS3 of bluetongue virus interferes with the induction of type I interferon. *J. Virol.* 2013, *87*, 8241–8246.

[43] Ruscanu, S., Pascale, F., Bourge, M., Hemati, B. et al., The double-stranded RNA bluetongue virus induces type I interferon in plasmacytoid dendritic cells via a MYD88-dependent TLR7/8-independent signaling pathway. *J. Virol.* 2012, *86*, 5817–5828.

[44] Schoggins, J. W., Wilson, S. J., Panis, M., Murphy, M. Y. et al., A diverse range of gene products are effectors of the type I interferon antiviral response. *Nature* 2011, *472*, 481–485.

[45] Sadler, A. J., Williams, B. R., Interferon-inducible antiviral effectors. *Nat. Rev. Immunol.* 2008, *8*, 559–568.

[46] Fensterl, V., Sen, G. C., Interferon-induced Ifit proteins: their role in viral pathogenesis. *J. Virol.* 2015, *89*, 2462–2468.

[47] Takahasi, K., Yoneyama, M., Nishihori, T., Hirai, R. et al., Nonself RNA-sensing mechanism of RIG-I helicase and activation of antiviral immune responses. *Mol. Cell.* 2008, *29*, 428–440.

[48] Maclachlan, N. J., Henderson, C., Schwartz-Cornil, I., Zientara, S., The immune response of ruminant livestock to bluetongue virus: from type I interferon to antibody. *Virus Res.* 2014, *182*, 71–77.

[49] Shuai, K., Liu, B., Regulation of JAK-STAT signalling in the immune system. *Nat. Rev. Immunol.* 2003, *3*, 900–911.

[50] Liu, N., Song, W., Wang, P., Lee, K. et al., Proteomics analysis of differential expression of cellular proteins in response to avian H9N2 virus infection in human cells. *Proteomics* 2008, *8*, 1851–1858.

[51] Alfonso, P., Rivera, J., Hernaez, B., Alonso, C., Escribano, J. M., Identification of cellular proteins modified in response to African swine fever virus infection by proteomics. *Proteomics* 2004, *4*, 2037–2046.

[52] Lu, W. T., Wilczynska, A., Smith, E., Bushell, M., The diverse roles of the eIF4A family: you are the company you keep. *Biochem. Soc. Trans.* 2014, *42*, 166–172.

[53] Garcia-Moreno, M., Sanz, M. A., Pelletier, J., Carrasco, L., Requirements for eIF4A and eIF2 during translation of Sindbis virus subgenomic mRNA in vertebrate and invertebrate host cells. *Cell. Microbiol.* 2013, *15*, 823–840.

[54] Schneider, U., Naegele, M., Staeheli, P., Schwemmle, M., Active borna disease virus polymerase complex requires a distinct nucleoprotein-to-phosphoprotein ratio but no viral X protein. *J. Virol.* 2003, *77*, 11781–11789.

[55] Gao, G., Luo, H., The ubiquitin-proteasome pathway in viral infections. *Can. J. Physiol. Pharmacol.* 2006, *84*, 5–14.

[56] Choi, A. G., Wong, J., Marchant, D., Luo, H., The ubiquitin-proteasome system in positive-strand RNA virus infection. *Rev. Med. Virol.* 2013, *23*, 85–96.

[57] Karpe, Y. A., Meng, X. J., Hepatitis E virus replication requires an active ubiquitin-proteasome system. *J. Virol.* 2012, *86*, 5948–5952.

[58] Widjaja, I., de Vries, E., Tscherne, D. M., Garcia-Sastre, A. et al., Inhibition of the ubiquitin-proteasome system affects influenza A virus infection at a postfusion step. *J. Virol.* 2010, *84*, 9625–9631.

[59] Satheshkumar, P. S., Anton, L. C., Sanz, P., Moss, B., Inhibition of the ubiquitin-proteasome system prevents vaccinia virus DNA replication and expression of intermediate and late genes. *J. Virol.* 2009, *83*, 2469–2479.

[60] Zhou, Y. J., Zhu, J. P., Zhou, T., Cheng, Q. et al., Identification of differentially expressed proteins in porcine alveolar macrophages infected with virulent/attenuated strains of porcine reproductive and respiratory syndrome virus. *PLoS One* 2014, *9*, e85767.

[61] Lopez, T., Silva-Ayala, D., Lopez, S., Arias, C. F., Replication of the rotavirus genome requires an active ubiquitin-proteasome system. *J. Virol.* 2011, *85*, 11964–11971.

[62] Hurt, E., Beck, M., Towards understanding nuclear pore complex architecture and dynamics in the age of integrative structural analysis. *Curr. Opin. Cell Biol.* 2015, *34*, 31–38.

[63] Amara, A., Mercer, J., Viral apoptotic mimicry. *Nat. Rev. Microbiol.* 2015, *13*, 461–469.

[64] Stewart, M. E., Roy, P., Role of cellular caspases, nuclear factor-kappa B and interferon regulatory factors in Bluetongue virus infection and cell fate. *Virol. J.* 2010, *7*, 362.

[65] Nagaleekar, V. K., Tiwari, A. K., Kataria, R. S., Bais, M. V. et al., Bluetongue virus induces apoptosis in cultured mammalian cells by both caspase-dependent extrinsic and intrinsic apoptotic pathways. *Arch. Virol.* 2007, *152*, 1751–1756.

[66] Shai, B., Schmukler, E., Yaniv, R., Ziv, N. et al., Epizootic hemorrhagic disease virus induces and benefits from cell stress, autophagy, and apoptosis. *J. Virol.* 2013, *87*, 13397–13408.

